Gated Ion Transport in a Soft Nanochannel with Biomimetic Polyelectrolyte Brush Layers

Can Zhou,[1,+] Lanju Mei,[1,+] Yen-Shao Su,[2] Li-Hsien Yeh,[2,*] Xiaoyu Zhang,[1,*]

and Shizhi Qian[1]

[1]Department of Mechanical and Aerospace Engineering, Old Dominion University,

Norfolk, VA 23529, USA

[2]Department of Chemical and Materials Engineering, National Yunlin University of Science and Technology, Yunlin 64002, Taiwan

+ These authors contributed equally to this work

* Corresponding authors:

Fax: +886-5-5312071; E-mail: lhyeh@yuntech.edu.tw (Li-Hsien Yeh),

x1zhang@odu.edu (Xiaoyu Zhang)

Abstract

Functionalized nanofluidics has recently emerged as a powerful platform for applications of energy conversion as well as ionic diodes. Inspired by biological cells, we theoretically investigate for the first time the gate modulation of ion transport and selectivity in the soft nanochannel functionalized with biomimetic, pH-tunable, zwitterionic polyelectrolyte (PE) brush layers. The gate effect on the modulation of Donnan potential, ionic conductance, and ion selectivity in the biomimetic soft nanochannel is remarkable when the background salt concentration is low, pH is close to the isoelectric point of PE brush layers (slightly acidic), and the grafting density of PE brushes on the channel wall is small. Under those conditions, the biomimetic gated soft nanochannel is capable of being highly cation-selective when a negative gate voltage is applied. The findings provide a novel way for designing nanofluidic devices used in osmotic energy conversion and ion current rectification.

Keywords: Nanofluidics; Nanochannel Conductance; Ion Selectivity; Donnan Potential; Field Effect Transistor

1. Introduction

Recently, chemically functionalized nanofluidics, solid-state nanochannels or nanopores decorated with functional polyelectrolyte (PE) brushes, has attracted increasing interests because of its implications for emerging areas such as ion current rectification [1-6], energy harvesting [7-9], electrochemical sensors [10, 11], and single (bio)nanoparticle sensing [12-14], to name a few. Such emerging potential is due to the significant overlapping of electric double layers (EDLs) in the functionalized nanofluidics. The liquid in such confined nanospace becomes charged, thus creating several unique and important phenomena, such as ion selectivity [15, 16] and surface-charge-governed ion transport behavior [17-19], which are not observed in the bulk state. The fundamental understanding of the physics behind these ion transport phenomena is essential for the development of functionalized nanofluidics. Despite the growing experimental and theoretical efforts, the understanding of the ion transport behaviors in functionalized nanofluidics remains limited. The difficulty, in addition to the significant EDL overlap effect, comes from the interfacial chemical reactions between the functional groups in PE chains and bonded ions (e.g., protons), taking account of which in the model will significantly increase the complexity of mathematical analysis.

Controlling the ion transport in nanofluidics is a key for the design of next generation nanofluidic devices. However, the surface charge properties and ion transport behaviors in the above-mentioned functionalized nanofluidics are passively and inherently determined by the solution properties (e.g., pH and salt concentration). This implies that active control of the ion transport in the functionalized nanofluidics is difficult. Recently, the nanofluidic field effect transistor (FET) [20-22], comprising a gate electrode embedded beneath the thin dielectric channel layer, has been developed. It has been demonstrated that the FET is capable of actively controlling the surface charge property and ionic conductance in a solid-state nanochannel and nanopore by controlling the gate voltage applied to the gate electrode

[23-34]. Compared to the large number of studies on the solid-state nanofluidic FET, Benson *et al.* [35] and Milne *et al.* [36] recently initiated the studies of the FET control of the Donnan potential, the electrical potential at the PE layer/solid channel interface [37], and the electrokinetic flow (EKF) in the functionalized soft nanochannels. The major difference between the solid-sate and the functionalized soft nanofluidics arises from the fact that the field effect control of ion transport in the former is dominated by the zeta potential at the solid channel wall [27, 30], while in the latter by the Donnan potential and the charge density of functionalized PE brush layers, which will be shown later. Benson *et al.* [35] and Milne *et al.* [36] demonstrated that by regulating the gate voltage, the Donnan potential and EKF in the soft nanochannel can be actively controlled. However, they only analyzed the fluid transport in the soft nanochannel and neglected the EDL overlap effect in their model. It is known that the ion transport is far more significant than the fluid transport in nanofluidic devices because the principle of nanofluidic sensors is based on analyzing the ionic current (or conductance) stemming from the transport of ions [38-40]. Moreover, as explained previously, the EDL overlap effect in functionalized soft nanofluidics is extremely significant. Neglecting the overlapping effect of EDLs, although makes the mathematic analyses much simpler, could yield incorrect estimation of the relevant transport behaviors in functionalized nanofluidics under the condition of overlapped EDLs.

In this study, the FET control of the ion transport and selectivity in a soft nanochannel functionalized with biomimetic, pH-tunable, zwitterionic PE brush layers is investigated for the first time. The study extends the previous analyses on the electrokinetic flow [35, 36] to the case of ion transport, which is more significant than the fluid transport in the nanofluidic applications. Moreover, the EDL overlap effect, which was neglected in previous studies [35, 36], is also taken into account in the present study. Through the comprehensive parametric studies, we show that the FET control of the charge property of PE brush layers, ionic

conductance, and ion selectivity in the biomimetic soft nanochannel depends apparently on the solution pH, salt concentration, and the grafting density of PE brushes on the channel wall.

2. Mathematical Model

Fig. 1 depicts the schematic view of the electrokinetic ion and fluid transports in a pH tunable soft nanochannel of height h, length L, and width W, gated by the FET comprising two thin dielectric channel layers of thickness d_c and the gate electrodes embedded outside those layers. The soft nanochannel comprises ion-penetrable, pH tunable, PE brush layers, which bear repeatable biomimetic zwitterionic functional constituents (e.g., lysine), $\mathrm{P} \sim \mathrm{COOH}$ and $\mathrm{P} \sim \mathrm{NH_2}$, of uniform thickness d_m on the both rigid channel walls. Suppose that the electric potential at the PE layer/channel wall interface is the well-known Donnan potential ϕ_d [37]. The electrokinetic transport in the soft nanochannel can be actively controlled by modulating ϕ_d through applying a gate voltage V_G to the gate electrode. The Cartesian coordinates, *y* and *z*, are adopted with the origin at the center of the soft nanochannel and a uniformly electric field of strength $E_z = V_0 / L$ is applied in the *z*-direction with V_0 being the voltage bias across the nanochannel.

For simplicity, we assume the following. (i) Both L and W are in microscale and only h is in nanoscale, implying that $L >> h$ and $W >> h$ and, therefore, the present problem can be regarded as a nanoslit. (ii) The PE layer is uniformly structured and the deformation of that layer is neglected, which is valid if the repeated unit of zwitterionic functional groups, N, is not too high (e.g., $N \le 20$) [41]. (iii) The relative permittivity, ε_f, and dynamic viscosity, η, of fluid and the diffusivity of the ionic species j, D_j, inside the PE brush layers are the same as those outside them. (iv) The ion concentration polarization effect [42, 43] in the nanochannel is neglected, which is valid for a long nanochannel under

consideration. (v) To simulate the experimental conditions, the ionic concentration of aqueous solution is controlled by the background salt, KCl, with adjustment of pH by HCl and KOH. Consequently, four major ionic species, including H^+, K^+, OH^- and Cl^-, need to be considered. Let C_{j0} ($j = 1$, 2, 3, and 4) be the concentration of these ions and C_b be the background concentration of KCl. Electroneutrality of the bulk solution results in $C_{10} = 10^{-(\mathrm{pH}-3)}$, $C_{30} = 10^{-(14-\mathrm{pH}-3)}$, $C_{20} = C_b$, and $C_{40} = C_b + 10^{-(\mathrm{pH}-3)} - 10^{-(14-\mathrm{pH}-3)}$ for $\mathrm{pH} \le 7$ ($C_{20} = C_b - 10^{-(\mathrm{pH}-3)} + 10^{-(14-\mathrm{pH}-3)}$ and $C_{40} = C_b$ for $\mathrm{pH} > 7$) [44].

The following verified governing equations are employed to describe the underlying physics for the electric potentials within the dielectric channel layer ($h/2 \le y \le h/2 + d_c$) and liquid ($0 \le y \le h/2$), ψ and φ, respectively, and the flow field in the considered soft nanochannel,

$$\frac{d^2\psi}{dy^2} = 0, \tag{1}$$

$$\frac{d^2\varphi}{dy^2} = -\frac{1}{\varepsilon_0 \varepsilon_f}\left[\sum_{j=1}^{4} F z_j C_{j0} \exp\left(-\frac{z_j \varphi}{\varphi_0}\right) + i\rho_m\right], \tag{2}$$

$$\frac{d^2 v}{dy^2} = -\frac{E_z}{\eta}\sum_{j=1}^{4} F z_j C_{j0} \exp\left(-\frac{z_j \varphi}{\varphi_0}\right) + \frac{iv}{(\lambda_m)^2}. \tag{3}$$

In the equations above, $i = 0$ and 1 denote the regions outside ($0 \le y \le h/2 - d_m$) and inside ($h/2 - d_m \le y \le h/2$) the PE layers; ε_0 and ε_f are the absolute permittivity of vacuum and the relative permittivity of liquid, respectively; z_j is the valence of the ionic species j; $\varphi_0 = RT/F$ is the reference thermal potential with R, T, and F being the universal gas constant, fluid temperature, and Faraday constant, respectively; v is the fully developed electrokinetic flow velocity in the z-direction; ρ_m is the volume charge density of PE brush

layers; $\lambda_m = \sqrt{\eta / \chi_m}$ and χ_m are the softness degree and hydrodynamic frictional coefficient of PE brush layers, respectively. Typically, λ_m is in the range from 0.1 to 10 nm for biological soft layers [45]. Note that Eq. (2) is suitable for describing the electric potential in the soft nanochannel under the condition of overlapped EDLs, which is proven in the detailed derivation in the Supplementary Data. The last term of Eq. (3) describes the influence of the softness of PE brushes on the flow field in the PE-modified nanochannel.

Suppose that the considered biomimetic zwitterionic functional groups, $\mathrm{P\sim COOH}$ and $\mathrm{P\sim NH_2}$, within the PE brush layers are capable of proceeding the deprotonation/protonation reactions, $\mathrm{P\sim COOH \leftrightarrow P\sim COO^- + H^+}$ and $\mathrm{P\sim NH_2 + H^+ \leftrightarrow P\sim NH_3^+}$, respectively. Let $K_a = [\mathrm{P\sim COO^-}][\mathrm{H^+}]/[\mathrm{P\sim COOH}]$ and $K_b = [\mathrm{P\sim NH_3^+}]/\left([\mathrm{P\sim NH_2}][\mathrm{H^+}]\right)$ be the equilibrium constants of these reactions, respectively. Here, $[\mathrm{H^+}] = 10^{-\mathrm{pH}} \exp\left(-\varphi/\varphi_0\right)$ denote the molar concentration of protons and the other brackets denote the volume site density of corresponding functional groups inside the bracket. It can be shown that the volume charge density of PE brush layers in Eq. (2) can be expressed as,

$$\rho_m = 1000F\left([\mathrm{P\sim NH_3^+}] - [\mathrm{P\sim COO^-}]\right) = 1000F\left(\frac{K_b\alpha_b[\mathrm{H^+}]}{1+K_b[\mathrm{H^+}]} - \frac{K_a\alpha_a}{K_a+[\mathrm{H^+}]}\right), \tag{4}$$

where $\alpha_a = [\mathrm{P\sim COO^-}] + [\mathrm{P\sim COOH}] = N\sigma_m / 1000 d_m n_a$ and $\alpha_b = [\mathrm{P\sim NH_3^+}] + [\mathrm{P\sim NH_2}] = N\sigma_m / 1000 d_m n_a$ are the net volume site density of acidic and basic functional groups; σ_m is the grafting density of PE brushes on the inner channel wall (typically ranging from 0.05 to 0.6 chains/nm^2) [6, 41, 46]; n_a is the Avogadro constant.

Assuming that the non-slip plane locates at the PE layer/channel wall interface ($y = h/2$) and its interfacial charged property is neutral, the boundary conditions for Eqs. (1)-(3) are

$$\psi = V_G \quad \text{at} \quad y = h/2 + d_c, \tag{5}$$

$$\psi = \varphi = \phi_d \quad \text{at} \quad y = h/2, \tag{6}$$

$$\varepsilon_d \frac{d\psi}{dy} = \varepsilon_f \frac{d\varphi}{dy} \quad \text{at} \quad y = h/2, \tag{7}$$

$$v = 0 \quad \text{at} \quad y = h/2, \tag{8}$$

$$\varphi\big|_{y=(h/2-d_m)^-} = \varphi\big|_{y=(h/2-d_m)^+}, \tag{9}$$

$$\left.\frac{d\varphi}{dy}\right|_{y=(h/2-d_m)^-} = \left.\frac{d\varphi}{dy}\right|_{y=(h/2-d_m)^+}, \tag{10}$$

$$v\big|_{y=(h/2-d_m)^-} = v\big|_{y=(h/2-d_m)^+}, \tag{11}$$

$$\left.\frac{dv}{dy}\right|_{y=(h/2-d_m)^-} = \left.\frac{dv}{dy}\right|_{y=(h/2-d_m)^+}, \tag{12}$$

$$\frac{d\varphi}{dy} = 0, \text{ at} \quad y = 0 \tag{13}$$

$$\frac{dv}{dy} = 0, \text{ at} \quad y = 0 \tag{14}$$

Here, ε_d is the relative permittivity of dielectric channel layers. Eq. (6) represents the electric potential at the PE layer/channel wall interface (i.e., Donnan potential, ϕ_d) is continuous, while the transverse electric field at that interface, as represented in Eq. (7), is discontinuous owing to the inconsistence of ε_d and ε_f. Eqs. (9)-(12) represent the electric potential, transverse electric field, and flow field are continuous at the liquid/PE layer interface. Equation 13 implies that the EDL overlap effect, which was typically neglected in previous similar studies by assuming $\varphi = 0$ [28, 35, 36], is taken into account in the present study.

Assuming that there is no external pressure and concentration-gradient fields applied across the soft nanochannel, the ionic current (I_{ch}) and conductance (G_{ch}) in the soft nanochannel can be estimated by [47]

$$I_{ch} = 2W\int_0^{\frac{h}{2}}\left(\sum_{j=1}^{4} Fz_j J_j\right)dy = 2W\left[\sum_{j=1}^{4}\int_0^{\frac{h}{2}}\left(vFz_j C_j\right)dy + \sum_{j=1}^{4}\int_0^{\frac{h}{2}}\left(\frac{F^2 V_0 D_j C_j}{RTL}\right)dy\right], \tag{15}$$

$$G_{ch} = I_{ch} / V_0, \tag{16}$$

where J_j is the flux of ionic species j and $C_j = C_{j0}\exp\left(-\frac{z_j\varphi}{\varphi_0}\right)$ is the concentration of ionic species j perpendicular to the charged soft nanochannel. The first and second terms in the right bracket of Eq. (15) represent the ionic current contributed from the convection (electrokinetic flow) and electromigration (applied electric field) terms, respectively. Once the ionic current stemming from the transport of all ionic species is obtained, the ion selectivity of the soft nanochannel can be calculated by [15, 16]

$$S_{ch} = \frac{\left|I_{ca}\right| - \left|I_{an}\right|}{\left|I_{ca}\right| + \left|I_{an}\right|}, \tag{17}$$

where $I_{ca} = 2W\int_0^{\frac{h}{2}}\left(\sum_{j=1}^{2} Fz_j J_j\right)dy$ and $I_{an} = 2W\int_0^{\frac{h}{2}}\left(\sum_{j=3}^{4} Fz_j J_j\right)dy$ represent the currents contributed from cations and anions, respectively. If $S_{ch} < 0$ ($S_{ch} > 0$), implying $\left|I_{ca}\right| < \left|I_{an}\right|$ ($\left|I_{ca}\right| > \left|I_{an}\right|$), the more apparent deviation of S_{ch} from 0 denotes the more apparent anions-selective (cations-selective) for the soft nanochannel.

To estimate the gate modulation effect on the charge property of considered biomimetic soft nanochannel, we define the volume-averaged charge density of PE brush layers as

$$\overline{\rho}_m = \frac{1}{d_m}\int_{\frac{h}{2}-d_m}^{\frac{h}{2}} \rho_m dy, \tag{18}$$

3. Results and Discussion

The model described above is implemented numerically by COMSOL Multiphysics (version 5.2). The numerical scheme has been validated to be sufficiently accurate for

capturing the underlying physics of the ion transport in similar soft nanopores without gate control [13, 14, 48, 49] and the EKF in gated soft nanochannels without considering the EDL overlap effect [35, 36]. Unless specified otherwise, we consider the biomimetic soft nanochannel with $L = 10\ \mu$m, $W = 10\ \mu$m, $h = 30$ nm, $d_c = 40$ nm, and the surface modification layers of amino acid-like zwitterionic PE brushes on the inner channel walls with $N = 20$, $d_m = 6$ nm, $\lambda_m = 1$ nm, $\sigma_m = 0.15$ chains/nm^2, $\mathrm{p}K_a = -\log K_a = 2.2$ (α-carboxyl), and $\mathrm{p}K_b = -\log K_b = -8.8$ (α-amino) [50]. The isoelectric point (IEP) of considered PE brush layers is 5.5. At $T = 298$ K, the other constant parameters are $\varepsilon_0 = 8.854 \times 10^{-12}$ CV^{-1}m^{-1}, $\varepsilon_f = 80$, $\varepsilon_d = 3.9$ (SiO_2) [51], $\eta = 10^{-3}$ Pa·s, and D_j ($j = 1$, 2, 3, and 4) $= 9.31$, 1.96, 5.30, and 2.03 ($\times 10^{-9}$) for H^+, K^+, OH^-, and Cl^- ions, respectively.

3.1 Model Validation

The code validation of the present model is examined by comparing its results with the analytical results of Ma *et al.* [30], who derived the ionic conductance (G_{ch}) in the gated solid-state nanochannel without considering the EDL overlap effect. To simulate the rigid surface of nanochannel without PE brush layers, we assume a very large value of $\lambda_m = 10^{10}$ nm, a very small value of $d_m = 0.1$ nm [36], $N = 1$, and $h = 300$ nm. Fig. 2 shows the salt concentration dependence on G_{ch} for two levels of V_G at $\mathrm{pH} = 8$. Note that under the considered background KCl concentration C_b ranging from $0.01 \sim 1000$ mM, the corresponding $\kappa h / 2$ ranges from 1.6 to 488.8, implying that the EDL overlap effect is insignificant. Fig. 2 clearly reveals that no matter if the FET is active ($V_G = -20$ V) or not ($V_G = 0$ V), our simulated results (symbols) are in excellent agreement with the analytical results of Ma *et al.* [30] (solid lines) in the entire range of C_b. Thus the implementation of

the present model has been validated. Note that the applicability of the adopted continuum model for the soft nanofluidics has been recently validated by Lin et al. [52], who used a similar model to fit the experimental data of ion current rectification in the PE-modified nanopore without consideration of the gate control.

3.2 Influence of Background Salt Concentration on the Gated Ion Transport

Fig. 3 depicts the variations of the Donnan potential ϕ_d, volume-averaged charge density of PE brush layers $\bar{\rho}_m$, conductance G_{ch}, and ion selectivity S_{ch} of the gated biomimetic soft nanochannel with the background KCl concentration C_b for various gate voltages V_G at $\mathrm{pH} = 7$. As expected, Fig. 3a and b shows that $\phi_d < 0$ and $\bar{\rho}_m < 0$ if the gate is floating (i.e., $V_G = 0$ V). This arises from the fact that if the solution pH is higher than the IEP of PE brush layers (i.e., 7 > 5.5), more negatively charged constituents ($\mathrm{P} \sim \mathrm{COO}^-$) are dissociated from the acidic functional groups ($\mathrm{P} \sim \mathrm{COOH}$). Moreover, $|\phi_d|$ decreases (Fig. 3a) but $|\bar{\rho}_m|$ (Fig. 3b) increases with increasing C_b. The former can be attributed to the more significant counterion condensation effect in the PE brush layers with thinner EDL thickness [53]. The latter is due to the fact that as the background KCl concentration increases, the amount of H^+ ions excluded by the other background cations (K^+) increases [53]. It results in a higher local pH within the PE brush layers and, therefore, a higher $|\bar{\rho}_m|$.

If the gate electrode is active (i.e., $V_G \neq 0$ V), Fig. 3a reveals that ϕ_d is tunable and $|\phi_d|$ increases with an increase in negative V_G, exhibiting an expected gate control behavior. However, as seen in Fig. 3b, $|\bar{\rho}_m|$ decreases with an increase in negative V_G if C_b is relatively high. This can be attributed to the reduction of local pH within the PE brush layers due to an increase in the attraction of H^+ ions by the increase of negative ϕ_d shown in Fig. 3a. Note that if C_b is sufficiently low, $\bar{\rho}_m$ changes its sign to positive and increases with

an increase in negative V_G (yellow region). The interesting phenomena arise from the fact that the more appreciable H^+ ions are attracted into the PE brush layers at lower concentration of background salt. In this case, the negative Donnan potential at the PE brush layer/solid channel interface increases appreciably at negative V_G applied to the gate electrode (Fig. 3a), yielding an apparently low local pH, which turns into smaller than their IEP, within the PE brush layers and, therefore, positive charge density of PE brush layers.

Fig. 3c shows that the dependence of G_{ch} on C_b, regardless of the levels of V_G, reveals a linear relationship at sufficiently high C_b and non-linear behavior at low C_b. The former is expected because if the salt concentration is high, the nanochannel conductance, showing a bulk conductance behavior, is primarily dominated by the ionic concentrations and the nanochannel geometry [38]. The later verifies the conventional surface-charge-dominated ionic conductance behavior, implying that the surface conductance becomes significant. In this case, the nanochannel conductance depends apparently on its surface charges. Therefore, if the gate electrode is turned on, the nanochannel conductance increases appreciably with an increase in negative gate voltage as shown in Fig. 3c.

Fig. 3d suggests that the nanochannel is cation-selective ($S_{ch} > 0$) for the considered range of C_b and negative V_G. This is consistent with the results of negative ϕ_d (Fig. 3a), but inconsistent with those of positive $\bar{\rho}_m$ when C_b is sufficiently low and the negative V_G is applied (yellow region in Fig. 3b). This implies that if the modulated $|\phi_d|$ is sufficiently large, the ion selectivity in the biomimetic soft nanochannel is majorly dominated by its Donnan potential at the PE brush layer/solid channel interface. However, it is difficult to measure the Donnan potential of soft nanochannels in experiments. The present model provides a convenient means for the estimation of the Donnan potential as well as for the interpretation of relevant ion transport phenomena in functionalized soft nanochannels. It

should be pointed out in Fig. 3d that if a negative V_G is applied, the biomimetic soft nanochannel becomes highly cation-selective (i.e., $S_{ch} \cong 1$) even at a relatively high background salt concentration. The feature suggests that the proposed biomimetic gated soft nanochannel has great potential implications for developing next-generation osmotic energy conversion devices, in which the energy conversion efficiency depends significantly on the ion selectivity of nanochannels [54-57].

To further explore the influence of the background KCl concentration, C_b, on the gate modulation behaviors in the biomimetic soft nanochannel, the variations of the Donnan potential ϕ_d, volume-averaged charge density of PE brush layers $\bar{\rho}_m$, conductance G_{ch}, and ion selectivity S_{ch} with the gate voltage V_G for various levels of C_b are plotted in Fig. 4. Fig. 4a reveals that ϕ_d is tunable with V_G and changes from negative to positive (pink region) if the positive V_G is sufficiently large. The performance of the gate modulation of ϕ_d is better at lower background salt concentration. This can be explained by the fact that the higher the salt concentration, the thinner the EDL thickness, yielding the more counterions confined into the PE brush layers and, therefore, making the gate harder to modulate the Donnan potential. Note that the salt dependence of ϕ_d at negative V_G is more appreciable than that at positive V_G. For example, the relative differences of ϕ_d between the results at $C_b = 0.1$ mM and 100 mM for $V_G = -10$ and -20 V are as large as 384 and 545 %, respectively, while those for $V_G = +10$ and $+20$ V are ca. 129 and 150 %. This implies that the background salt plays a more notable role on the gate modulation of ϕ_d if a negative gate voltage is applied.

Fig. 4b shows that if C_b is sufficiently high, $\bar{\rho}_m$ under the considered range of V_G is all negative and $|\bar{\rho}_m|$ increases with the variation of V_G from -20 to 20 V. This can be

explained by the gate modulation of ϕ_d shown in Fig. 4a and attributed to the depleted local concentration of H^+ ions (an increase in the local pH) within the PE brush layers with variation of V_G. If C_b is extremely low, $\bar{\rho}_m$ turns from negative to positive if the negative V_G is sufficiently large, which can be explained by the same reasoning employed in Fig. 3b. Similar to the results depicted in Fig. 3a and b, the gate modulation behaviors of ϕ_d and $\bar{\rho}_m$ in Fig. 4a and b are distinctly different.

Fig. 4c shows that if C_b is high, G_{ch} is almost independent of V_G, while becomes highly tunable with V_G if C_b is sufficiently low. The former emerges the bulk conductance behavior. The latter is quite interesting since at low salt concentration, the nanochannel conductance becomes highly dependent on its surface charges and the gate modulation of Donnan potential is significant (Fig. 4a), yielding the advantageous performance of the gated ion transport. It is interesting to note in Fig. 4c that the salt dependence of G_{ch} at negative V_G is less significant than that at positive V_G, which is in contrast to that dependence of ϕ_d shown in Fig. 4a. For example, the relative differences of G_{ch} between the results at $C_b = 0.1$ mM and 100 mM for $V_G = -10$ and -20 V are as large as 34.5 and 17.2 times, respectively, while those for $V_G = +10$ and $+20$ V are ca. 958 and 839 times. This is because as the background salt concentration increases, the magnitude of Donnan potential for negative gate voltage increases more appreciably than that for positive gate voltage. Consequently, if the gate voltage is negative, the amount of counterions attracted into the nanochannel and, hence, the nanochannel conductance increases more tremendously with decreasing salt concentration. This also explains why a saturated conductance behavior takes place at low regime of background salt concentration if a negative gate voltage is applied, as shown in Fig. 3c.

Fig. 4d shows that regardless of the levels of C_b, the nanochannel is cation-selective ($S_{ch} > 0$) if the negative V_G is applied, while becomes anion-selective ($S_{ch} < 0$, pink region) if the sufficiently large positive V_G is applied. Comparing the gate modulation of ϕ_d, $\overline{\rho}_m$, and S_{ch} depicted in Fig. 4a, b, and d, respectively, shows again that if the modulated $|\phi_d|$ is sufficiently large, the behavior of S_{ch} is dominated firstly by that of ϕ_d, not $\overline{\rho}_m$. The gate modulation of ion selectivity of the biomimetic soft nanochannel is apparent at low background salt concentration.

3.3. Influence of Solution pH on the Gated Ion Transport

Fig. 5 depicts the variations of the Donnan potential ϕ_d, volume-averaged charge density of PE brush layers $\overline{\rho}_m$, conductance G_{ch}, and ion selectivity S_{ch} of the gated biomimetic soft nanochannel with pH for various gate voltages V_G at the background KCl concentration $C_b = 1$ mM. As shown in Fig. 5a and b, if the gate is floating at $V_G = 0$ V, $\phi_d > 0$ and $\overline{\rho}_m > 0$ ($\phi_d < 0$ and $\overline{\rho}_m < 0$) when pH < 5.5 (pH > 5.5). Moreover, Fig. 5a reveals that if the deviation of pH from 5.5 is not too large, $|\phi_d|$ increases as pH deviates from 5.5, and shows a local maximum as pH increases if pH is extremely high. The local maximum of $|\phi_d|$ with pH can be attributed to the apparent increase in the ionic strength due to the promotion of OH^- ions at extremely high pH regime [47]. It is worth noting in Fig. 5b that regardless of the values of pH, $|\overline{\rho}_m|$ monotonically increases with the deviation of pH from 5.5, which is inconsistent with the behavior of ϕ_d. This implies that the Donnan potential of biomimetic soft nanochannel depends both on pH and the net ionic strength, but the charge density of PE brush layers is only dominated by the former.

If the gate control is turned on (i.e., $V_G \neq 0$ V), Fig. 5a shows that $|\phi_d|$ increases with an

increase in negative V_G, which is expected. On the other hand, Fig. 5b shows that for $\bar{\rho}_m > 0$ ($\bar{\rho}_m < 0$), $\bar{\rho}_m$ increases ($|\bar{\rho}_m|$ decreases) as negative V_G increases. This can be explained by the same reasoning employed in Figs. 2b and 3b. The local concentration of H^+ ions within the PE brush layers increases with an increase in negative V_G, yielding a lower local pH and, therefore, more positively charged $P \sim NH_3^+$ groups (less negatively charged $P \sim COO^-$) formed if the local pH is lower (higher) than the IEP of PE brush layers. It should be pointed out in Fig. 5a that the gate control on ϕ_d is significant when pH is close to the IEP of PE brush layers (i.e., 5.5) and becomes worse when pH is extremely low and high. The latter can be attributed to higher ionic strength of solution,

Fig. 5c reveals that regardless of the levels of V_G, G_{ch} shows a local minimum as pH varies. This can be attributed to the consequence of the following reasons: (i) the increase in the ionic strength with deviation of pH from neutrality, (ii) the apparently higher mobility of H^+ and OH^- ions than other background K^+ and Cl^- ions, which becomes dominant when pH is extremely low and high, and (iii) the relatively larger magnitude of ϕ_d when pH is extremely low and high. Fig. 5c also suggests that the performance of the gate modulation of G_{ch} is notable at medium pH, and becomes trivial when pH apparently deviates from neutrality. This can be attributed to the significant increase in the ionic strength of solution at extremely low and high pH, leading to a thinner EDL thickness and, therefore, less significant surface-charge-dominated ion transport behavior.

Fig. 5d shows that when pH is sufficiently high, $S_{ch} \cong 1$ (nearly fully cation-selective) no matter if the gate control is closed ($V_G = 0$ V) or opened ($V_G \neq 0$ V), originating from the significantly large negative ϕ_d shown in Fig. 5a. For lower pH, the gate modulation of positive S_{ch} decreases as pH decreases, and changes its sign to negative when pH becomes

sufficiently low. This can be majorly attributed to the gate modulation of ϕ_d seen in Fig. 5a. Fig. 5d also reveals that when pH is extremely low, the negative S_{ch} goes through a local maximum as pH decreases. This arises from the significantly high bulk concentration of H^+ ions at extremely low pH, which contributes appreciably to the cation current, I_{ca}, thus reducing the degree of anion-selectivity. Note that the gate modulation performance of S_{ch} is better when pH is close to the IEP of PE brush layers, which is consistent with the result of modulated ϕ_d seen in Fig. 5a. Owing to the highly tunable ϕ_d for $5.5 < \mathrm{pH} < 7$, S_{ch} jumps up close to unity, implying that the nanochannel becomes highly cation-selective, when the gate control is turned on ($V_G < 0$ V). This implies that under the solution pH in the typical environment (typically slightly acidic), the gated biomimetic soft nanochannel still has great potential in the application of osmotic energy harvesting [54-57].

The influence of pH on the gate modulation behaviors in the biomimetic soft nanochannel is further discussed in Fig. 6, where the variations of ϕ_d, $\bar{\rho}_m$, G_{ch}, and S_{ch} with V_G for three levels of pH are presented. Fig. 6a indicates that in addition to pH, the sign of Donnan potential can be controlled by the gate voltage, showing the typical gate control behavior. Fig. 6b reveals that $\bar{\rho}_m > 0$ for $\mathrm{pH} = 3.5$, while $\bar{\rho}_m < 0$ for $\mathrm{pH} = 7.5$ and 10. If $\bar{\rho}_m < 0$, the magnitude of $\bar{\rho}_m$ increases with the variation of V_G, but decreases with V_G if $\bar{\rho}_m > 0$. Again, this can be attributed to the exclusion effect of H^+ ions mentioned in Fig. 5b. Fig. 6c suggests that the gate modulation of G_{ch} depends on the solution pH. For example, for $\mathrm{pH} = 7.5$ and 10, G_{ch} decreases with the variation of V_G, but increases with V_G for $\mathrm{pH} = 3.5$. As shown previously, the nanochannel conductance at $C_b = 1$ mM lies in the surface-charge-dominated region. Therefore, the pH dependence of modulated G_{ch} seen in Fig. 6c can be explained by the behavior of ϕ_d depicted in Fig. 6a. Fig. 6d suggests that for

higher $\mathrm{pH} = 7.5$ and 10, $S_{ch} > 0$ (cation-selective) and decreases monotonically as V_G varies from -20 to 20 V. On the other hand, for lower $\mathrm{pH} = 3.5$, S_{ch} becomes negative (pink region) and its magnitude increases monotonically with V_G. The most interesting phenomenon is that for $\mathrm{pH} = 7.5$ ($\mathrm{pH} = 3.5$), the nanochannel is still cation-selective (anion-selective), even though the sign of its modulated Donnan potential is changed (see Fig. 6a), when the sufficiently large positive (negative) V_G is applied. This apparently implies that if the magnitude of the modulated ϕ_d, the sign of which is reversed from the original charge nature, is not sufficiently large, the sign of the ion selectivity in the biomimetic gated soft nanochannel is dominated by the negative (positive) charge density of PE brush layers, at sufficiently large positive (negative) V_G for $\mathrm{pH} = 7.5$ ($\mathrm{pH} = 3.5$).

3.4 Influence of Grafting Density of PE Brushes on the Gated Ion Transport

Fig. 7 summarizes the influence of the grafting density of PE brushes, σ_m, on the gate modulation of the Donnan potential ϕ_d, volume-averaged charge density of PE brush layers $\bar{\rho}_m$, conductance G_{ch}, and ion selectivity S_{ch} at $C_b = 1$ mM and $\mathrm{pH} = 7$. Note that under $\mathrm{pH} = 7$ (> IEP of PE brush layers), the Donnan potential (Fig. 7a) and the charge density of PE brush layers (Fig. 7b) at various values of σ_m are all negative for the soft nanochannel without gate control (i.e., $V_G = 0$ V). If the gate control is opened ($V_G \neq 0$ V), ϕ_d can be regulated from negative to positive (pink region) when V_G is sufficiently large (Fig. 7a), but $\bar{\rho}_m$ does not change its sign and its magnitude increases as V_G varies from -20 to 20 V (Fig. 7b). It is worth noting that the gate modulation of ϕ_d (Fig. 7a) and $\bar{\rho}_m$ (Fig. 7b) is more superior for smaller and larger σ_m, respectively. This is due to the fact that the larger the σ_m, the larger the charge density of PE brush layers, which attracts more counterions into the PE brush layers and makes the gate electrode harder to tune the Donnan potential.

Meanwhile, it is known that the charge density of PE brush layers depends highly on the local concentration of H^+ ions within that layer. Because the greater amount of counterions is confined into the PE brush layers for larger grafting density of PE brushes, it is much easier to tune the charge density of those layers.

Fig. 7c reveals that the performance of gate modulation of G_{ch} is better for smaller σ_m, which is consistent with that of ϕ_d seen in Fig. 7a since the ionic conductance in the soft nanochannel as mentioned previously is dominated primarily by its Donnan potential. Moreover, for smaller $\sigma_m = 0.1$ chains/nm^2, G_{ch} shows a local minimum as V_G varies from -20 to 20 V and the local minimum behavior disappears when σ_m gets larger. The local minimum of G_{ch} with the variation of V_G stems from the consequent result of the decrease in the negative ϕ_d and the further increase in the positive ϕ_d as V_G varies from -20 to 20 V shown in Fig. 7a. Because the magnitude of the reversed positive ϕ_d modulated by the gate electrode under the considered V_G is less appreciable for larger σ_m, the increase of G_{ch} with V_G at sufficiently large V_G vanishes.

Fig. 7d shows that the gate modulation of S_{ch} is more superior for smaller σ_m, which is in accordance with that of ϕ_d seen in Fig. 7a. Moreover, if σ_m is large, the nanochannel is cation-selective ($S_{ch} > 0$) under the entire range of V_G. However, if σ_m is sufficiently small, the nanochannel becomes anion-selective ($S_{ch} < 0$, pink region) when the sufficiently large V_G is applied. This clearly shows again that if the magnitude of the modulated ϕ_d, which has different sign from its origin one, is (is not) sufficiently large, the ion selectivity of the biomimetic soft nanochannel is majorly dominated by its modulated Donnan potential (charge density of PE brush layers).

4. Conclusions

In summary, a multi-ion model that includes the electrokinetic flow, electric double layers (EDLs) overlap, interfacial chemical reactions between the polyelectrolyte (PE) chains and protons has been developed to investigate the gate modulation of ion transport and selectivity in a soft nanochannel functionalized with biomimetic, pH-tunable, zwitterionic PE brush layers. The results demonstrate that the Donnan potential, ionic conductance, and ion selectivity in the biomimetic soft nanochannel are capable of being highly tunable when the background salt concentration is low, pH is close to the isoelectric point (IEP) of PE brush layers (slightly acidic), and the grafting density of PE brushes on the channel wall is small. Because the charge density of PE brush layers is highly related to the local proton concentration inside those layers, the signs of the Donnan potential and the charge density of PE brush layers could be different if a significantly large negative or positive gate voltage is applied. If the magnitude of the modulated Donnan potential, the sign of which is opposite to its original one, is (is not) sufficiently large, the ion selectivity of the biomimetic soft nanochannel is dominated by its modulated Donnan potential (charge density of PE brush layers).

Acknowledgements

This work is supported by the Ministry of Science and Technology of the Republic of China under Grants MOST 102-2221-E-224-052-MY3 and 103-2221-E-224-039-MY3 (L.H.Y.), NSF CMMI-1265785 (S.Q.) and the China Scholarship Council (L.M.).

References

[1] M. Ali, P. Ramirez, S. Mafe, R. Neumann, W. Ensinger, A pH-Tunable Nanofluidic Diode with a Broad Range of Rectifying Properties, ACS Nano, 3 (2009) 603-8.

[2] B. Yameen, M. Ali, R. Neumann, W. Ensinger, W. Knoll, O. Azzaroni, Single Conical Nanopores Displaying pH-Tunable Rectifying Characteristics. Manipulating Ionic Transport With Zwitterionic Polymer Brushes, J Am Chem Soc, 131 (2009) 2070-1.

[3] X. Hou, Y.J. Liu, H. Dong, F. Yang, L. Li, L. Jiang, A pH-Gating Ionic Transport Nanodevice: Asymmetric Chemical Modification of Single Nanochannels, Adv Mater, 22 (2010) 2440-3.

[4] M. Ali, P. Ramirez, H.Q. Nguyen, S. Nasir, J. Cervera, S. Mafe, et al., Single Cigar-Shaped Nanopores Functionalized with Amphoteric Amino Acid Chains: Experimental and Theoretical Characterization, ACS Nano, 6 (2012) 3631-40.

[5] S.F. Buchsbaum, G. Nguyen, S. Howorka, Z.S. Siwy, DNA-Modified Polymer Pores Allow pH- and Voltage-Gated Control of Channel Flux, J Am Chem Soc, 136 (2014) 9902-5.

[6] M. Tagliazucchi, Y. Rabin, I. Szleifer, Transport Rectification in Nanopores with Outer Membranes Modified with Surface Charges and Polyelectrolytes, ACS Nano, 7 (2013) 9085-97.

[7] S. Chanda, S. Sinha, S. Das, Streaming Potential and Electroviscous Effects in Soft nanochannels: Towards Designing More Efficient Nanofluidic Electrochemomechanical Energy Converters, Soft Matter, 10 (2014) 7558-68.

[8] G. Chen, S. Das, Streaming Potential and Electroviscous Effects in Soft Nanochannels Beyond Debye-Huckel Linearization, J Colloid Interface Sci, 445 (2015) 357-63.

[9] Z. Zhang, X.Y. Kong, K. Xiao, Q. Liu, P. Li, J. Ma, et al., Engineered Asymmetric Heterogeneous Membrane: A Concentration-Gradient-Driven Energy Harvesting Device, J Am Chem Soc, 137 (2015) 14765-72.

[10] M. Lepoitevin, G. Nguyen, M. Bechelany, E. Balanzat, J.M. Janot, S. Balme, Combining a Sensor and a pH-Gated Nanopore Based on an Avidin-Biotin System, Chem Commun, 51 (2015) 5994-7.

[11] Z.M. Chen, G.Z. Shen, Y.P. Li, P. Zhang, H.W. Ji, S.C. Liu, et al., A Novel Biomimetic Logic Gate for Sensitive and Selective Detection of Pb(II) Base on Porous Alumina Nanochannels, Electrochem Commun, 60 (2015) 83-7.

[12] E.C. Yusko, J.M. Johnson, S. Majd, P. Prangkio, R.C. Rollings, J.L. Li, et al., Controlling Protein Translocation through Nanopores with Bio-Inspired Fluid Walls, Nat Nanotechnol, 6 (2011) 253-60.

[13] L.H. Yeh, M. Zhang, S. Qian, J.P. Hsu, Regulating DNA Translocation through Functionalized Soft Nanopores, Nanoscale, 4 (2012) 2685-93.

[14] L.H. Yeh, M.K. Zhang, S.W. Joo, S. Qian, J.P. Hsu, Controlling pH-Regulated Bionanoparticles Translocation through Nanopores with Polyelectrolyte Brushes, Anal Chem, 84 (2012) 9615-22.

[15] I. Vlassiouk, S. Smirnov, Z. Siwy, Ionic Selectivity of Single Nanochannels, Nano Lett, 8 (2008) 1978-85.

[16] L.H. Yeh, C. Hughes, Z. Zeng, S. Qian, Tuning Ion Transport and Selectivity by a Salt Gradient in a Charged Nanopore, Anal Chem, 86 (2014) 2681-6.

[17] D. Stein, M. Kruithof, C. Dekker, Surface-Charge-Governed Ion Transport in Nanofluidic Channels, Phys Rev Lett, 93 (2004) 035901.

[18] Z. Zeng, L.H. Yeh, M. Zhang, S. Qian, Ion Transport and Selectivity in Biomimetic Nanopores with pH-Tunable Zwitterionic Polyelectrolyte Brushes, Nanoscale, 7 (2015) 17020-9.

[19] M. Taghipoor, A. Bertsch, P. Renaud, An Improved Model for Predicting Electrical Conductance in Nanochannels, Phys Chem Chem Phys, 17 (2015) 4160-7.

[20] R. Karnik, R. Fan, M. Yue, D.Y. Li, P.D. Yang, A. Majumdar, Electrostatic Control of Ions and Molecules in Nanofluidic Transistors, Nano Lett, 5 (2005) 943-8.
[21] W.H. Guan, S.X. Li, M.A. Reed, Voltage Gated Ion and Molecule Transport in Engineered Nanochannels: Theory, Fabrication and Applications, Nanotechnology, 25 (2014) 122001.
[22] N. Hu, Y. Ai, S.Z. Qian, Field Effect Control of Electrokinetic Transport in Micro/Nanofluidics, Sens Actuator B: Chem, 161 (2012) 1150-67.
[23] J. Matovic, N. Adamovic, F. Radovanovic, Z. Jaksic, U. Schmid, Field Effect Transistor Based on Ions as Charge Carriers, Sens Actuator B: Chem, 170 (2012) 137-42.
[24] K.P. Singh, M. Kumar, Effect of Gate Length and Dielectric Thickness on Ion and Fluid Transport in a Fluidic Nanochannel, Lab Chip, 12 (2012) 1332-9.
[25] Y.H. He, M. Tsutsui, C. Fan, M. Taniguchi, T. Kawai, Controlling DNA Translocation through Gate Modulation of Nanopore Wall Surface Charges, ACS Nano, 5 (2011) 5509-18.
[26] S. Mafe, J.A. Manzanares, P. Ramirez, Gating of Nanopores: Modeling and Implementation of Logic Gates, J Phys Chem C, 114 (2010) 21287-90.
[27] L.H. Yeh, Y. Ma, S. Xue, S.Z. Qian, Gate Manipulation of Ionic Conductance in a Nanochannel with Overlapped Electric Double Layers, Sens Actuator B-Chem, 215 (2015) 266-71.
[28] L.H. Yeh, S. Xue, S.W. Joo, S. Qian, J.P. Hsu, Field Effect Control of Surface Charge Property and Electroosmotic Flow in Nanofluidics, J Phys Chem C, 116 (2012) 4209-16.
[29] C. Hughes, L.H. Yeh, S. Qian, Field Effect Modulation of Surface Charge Property and Electroosmotic Flow in a Nanochannel: Stern Layer Effect, J Phys Chem C, 117 (2013) 9322-31.
[30] Y. Ma, S. Xue, S.C. Hsu, L.H. Yeh, S. Qian, H. Tan, Programmable Ionic Conductance in a pH-Regulated Gated Nanochannel, Phys Chem Chem Phys, 16 (2014) 20138-46.
[31] G. Pardon, W. van der Wijngaart, Modeling and Simulation of Electrostatically Gated Nanochannels, Adv Colloid Interface Sci, 199 (2013) 78-94.
[32] W.H. Guan, R. Fan, M.A. Reed, Field-Effect Reconfigurable Nanofluidic Ionic Diodes, Nat Commun, 2 (2011) 506.
[33] S.H. Lee, H. Lee, T. Jin, S. Park, B.J. Yoon, G.Y. Sung, et al., Sub-10 nm Transparent All-Around-Gated Ambipolar Ionic Field Effect Transistor, Nanoscale, 7 (2015) 936-46.
[34] Y. Youn, S. Han, Investigation of Field Effects in a Solid-State Nanopore Transistor, Phys Chem Chem Phys, 17 (2015) 27806-11.
[35] L. Benson, L.H. Yeh, T.H. Chou, S. Qian, Field Effect Regulation of Donnan Potential and Electrokinetic Flow in a Functionalized Soft Nanochannel, Soft Matter, 9 (2013) 9767-73.
[36] Z. Milne, L.H. Yeh, T.H. Chou, S. Qian, Tunable Donnan Potential and Electrokinetic Flow in a Biomimetic Gated Nanochannel with pH-Regulated Polyelectrolyte Brushes, J Phys Chem C, 118 (2014) 19806-13.
[37] H. Ohshima, Electrophoresis of Soft Particles, Adv Colloid Interface Sci, 62 (1995) 189-235.
[38] R.B. Schoch, J.Y. Han, P. Renaud, Transport Phenomena in Nanofluidics, Rev Mod Phys, 80 (2008) 839-83.
[39] X. Hou, W. Guo, L. Jiang, Biomimetic Smart Nanopores and Nanochannels, Chem Soc Rev, 40 (2011) 2385-401.
[40] D.G. Haywood, Z.D. Harms, S.C. Jacobson, Electroosmotic Flow in Nanofluidic Channels, Anal Chem, 86 (2014) 11174-80.
[41] M. Tagliazucchi, Y. Rabin, I. Szleifer, Ion Transport and Molecular Organization Are Coupled in Polyelectrolyte-Modified Nanopores, J Am Chem Soc, 133 (2011) 17753-63.
[42] L.H. Yeh, M. Zhang, S. Qian, J.P. Hsu, S. Tseng, Ion Concentration Polarization in

Polyelectrolyte-Modified Nanopores, J Phys Chem C, 116 (2012) 8672-7.
[43] M. Jia, T. Kim, Multiphysics Simulation of Ion Concentration Polarization Induced by Nanoporous Membranes in Dual Channel Devices, Anal Chem, 86 (2014) 7360-7.
[44] L.H. Yeh, Y. Ma, S. Xue, S. Qian, Electroviscous Effect on the Streaming Current in a pH-Regulated Nanochannel, Electrochem Commun, 48 (2014) 77-80.
[45] J.F.L. Duval, F. Gaboriaud, Progress in Electrohydrodynamics of Soft Microbial Particle Interphases, Curr Opin Colloid Interface Sci, 15 (2010) 184-95.
[46] O. Peleg, M. Tagliazucchi, M. Kroger, Y. Rabin, I. Szleifer, Morphology Control of Hairy Nanopores, ACS Nano, 5 (2011) 4737-47.
[47] Y. Ma, L.H. Yeh, C.Y. Lin, L.J. Mei, S.Z. Qian, pH-Regulated Ionic Conductance in a Nanochannel with Overlapped Electric Double Layers, Anal Chem, 87 (2015) 4508-14.
[48] L.H. Yeh, M. Zhang, N. Hu, S.W. Joo, S. Qian, J.P. Hsu, Electrokinetic Ion and Fluid Transport in Nanopores Functionalized by Polyelectrolyte Brushes, Nanoscale, 4 (2012) 5169-77.
[49] Z. Zeng, Y. Ai, S. Qian, pH-Regulated Ionic Current Rectification in Conical Nanopores Functionalized with Polyelectrolyte brushes, Phys Chem Chem Phys, 16 (2014) 2465-74.
[50] R. Switzer, L. Garrity, Experimental Biochemistry, New York, USA: W. H. Freeman Publishing; 1999.
[51] Y. Ai, J. Liu, B.K. Zhang, S. Qian, Field Effect Regulation of DNA Translocation through a Nanopore, Anal Chem, 82 (2010) 8217-25.
[52] J.Y. Lin, C.Y. Lin, J.P. Hsu, S. Tseng, Ionic Current Rectification in a pH-Tunable Polyelectrolyte Brushes Functionalized Conical Nanopore: Effect of Salt Gradient, Anal Chem, (2016) DOI: 10.1021/acs.analchem.5b03074.
[53] L.H. Yeh, Y.H. Tai, N. Wang, J.P. Hsu, S. Qian, Electrokinetics of pH-Regulated Zwitterionic Polyelectrolyte Nanoparticles, Nanoscale, 4 (2012) 7575-84.
[54] D.K. Kim, C.H. Duan, Y.F. Chen, A. Majumdar, Power Generation from Concentration Gradient by Reverse Electrodialysis in Ion-Selective Nanochannels, Microfluid Nanofluid, 9 (2010) 1215-24.
[55] W. Guo, L.X. Cao, J.C. Xia, F.Q. Nie, W. Ma, J.M. Xue, et al., Energy Harvesting with Single-Ion-Selective Nanopores: A Concentration-Gradient-Driven Nanofluidic Power Source, Adv Funct Mater, 20 (2010) 1339-44.
[56] A. Siria, P. Poncharal, A.L. Biance, R. Fulcrand, X. Blase, S.T. Purcell, et al., Giant Osmotic Energy Conversion Measured in a Single Transmembrane Boron Nitride Nanotube, Nature, 494 (2013) 455-8.
[57] L.X. Cao, W. Guo, W. Ma, L. Wang, F. Xia, S.T. Wang, et al., Towards Understanding the Nanofluidic Reverse Electrodialysis System: Well Matched Charge Selectivity and Ionic Composition, Energy Environ Sci, 4 (2011) 2259-66.

Figure Captions

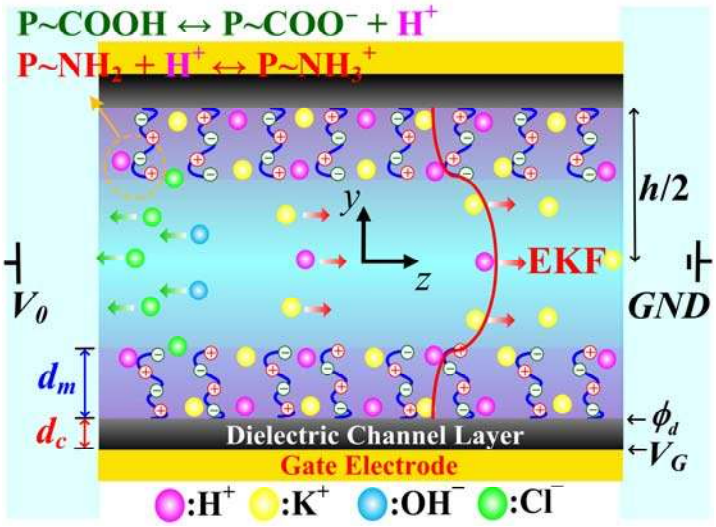

Fig. 1. Schematic illustration of the gate modulation of ion and fluid transports in a soft (e.g., negatively charged) nanochannel functionalized with biomimetic, pH-tunable, zwitterionic PE brush layers. The nanochannel is filled with electrolyte solution containing multiple H^+, K^+, OH^- and Cl^- ions. V_G is the gate voltage applied to the gate electrode, which is used to control the Donnan potential (ϕ_d) at the PE brush layer/solid channel interface, and the EKF and ion transport in the soft nanochannel.

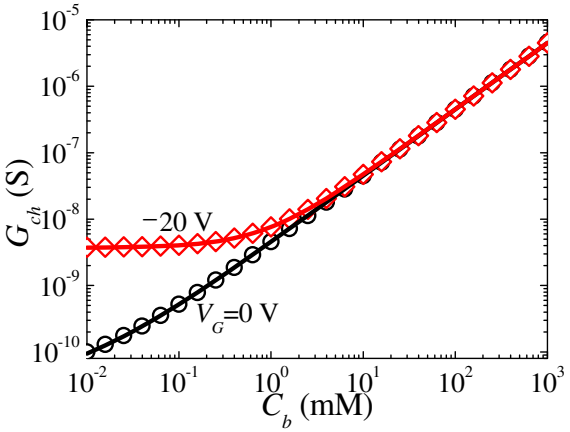

Fig. 2. Dependence of the nanochannel conductance, G_{ch}, on the background KCl concentration, C_b, for two values of V_G at $\mathrm{pH}=8$, $N=1$, $\lambda_m=10^{10}$ nm, $d_m=0.1$ nm, and $h=300$ nm. Circles and diamonds denote the present results at $V_G=0$ (floating gate) and −20 V (gate control), respectively. Solid lines denote the analytical results of Ma *et al.* [30].

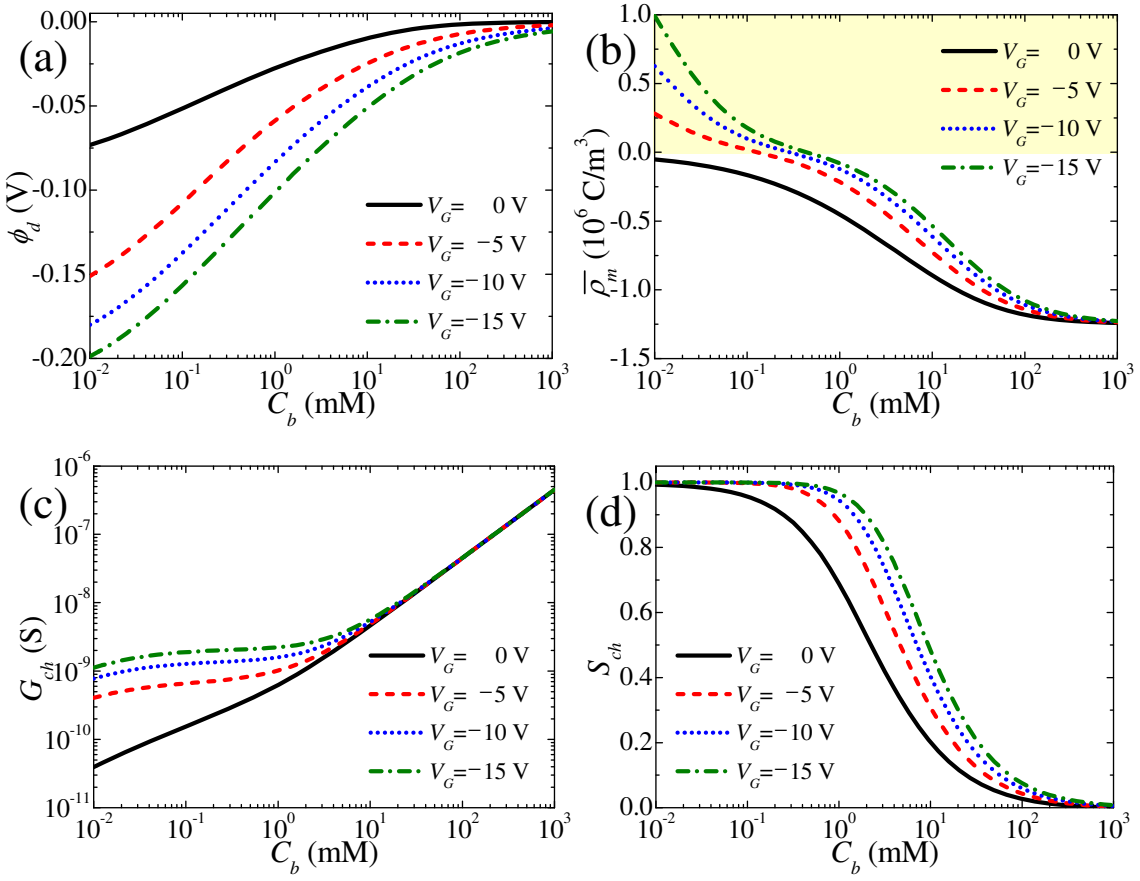

Fig. 3. Donnan potential ϕ_d, (a), volume-averaged charge density of PE brush layers $\overline{\rho}_m$, (b), conductance G_{ch}, (c), and ion selectivity S_{ch}, (d), as a function of the background KCl concentration C_b for various applied gated voltages V_G at $\mathrm{pH} = 7$. The yellow region in (b) highlights where the charge nature of PE brush layers changes.

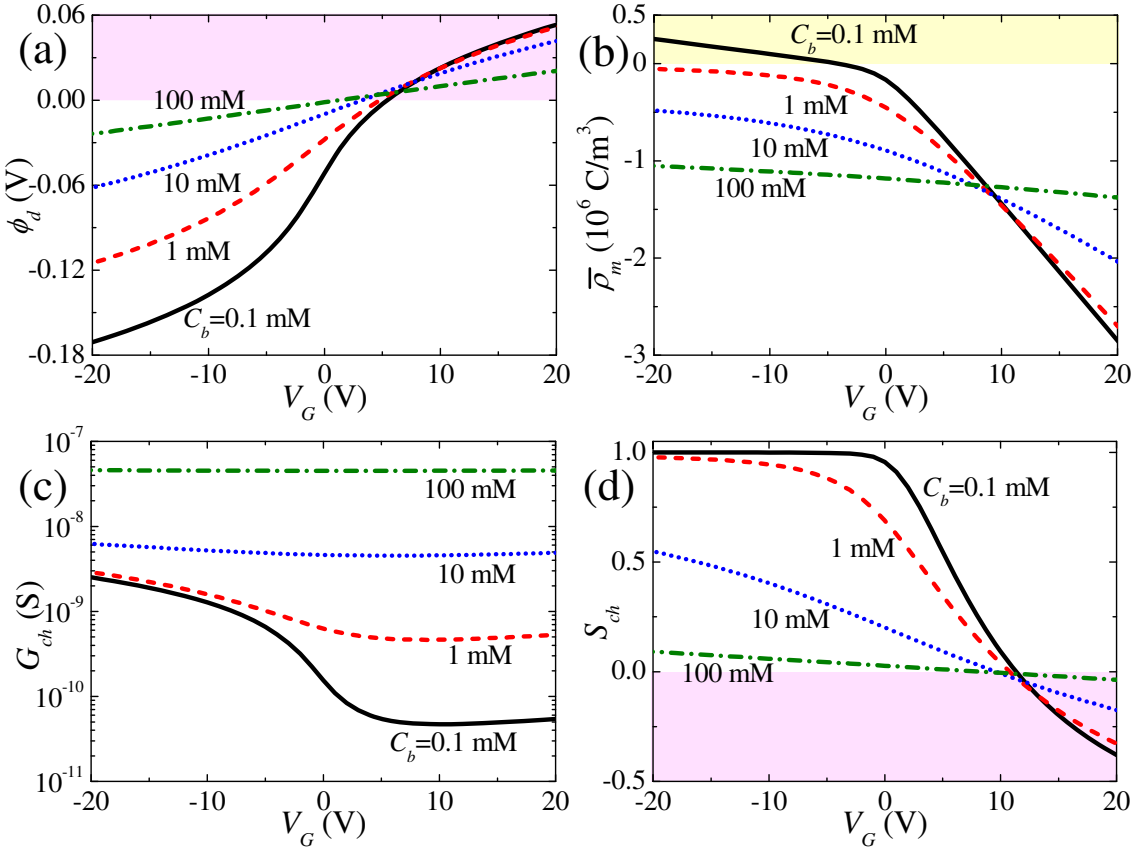

Fig. 4. Gate modulation of the Donnan potential ϕ_d, (a), volume-averaged charge density of PE brush layers $\overline{\rho}_m$, (b), conductance G_{ch}, (c), and ion selectivity S_{ch}, (d), as a function of the applied gated voltage V_G for various background KCl concentrations C_b at $\mathrm{pH}=7$. The yellow region in (b) highlights where the charge nature of PE brush layers changes. The pink regions in (b) and (d) highlight the reversal Donnan potential and ion selectivity of considered biomimetic gated soft nanochannel, respectively.

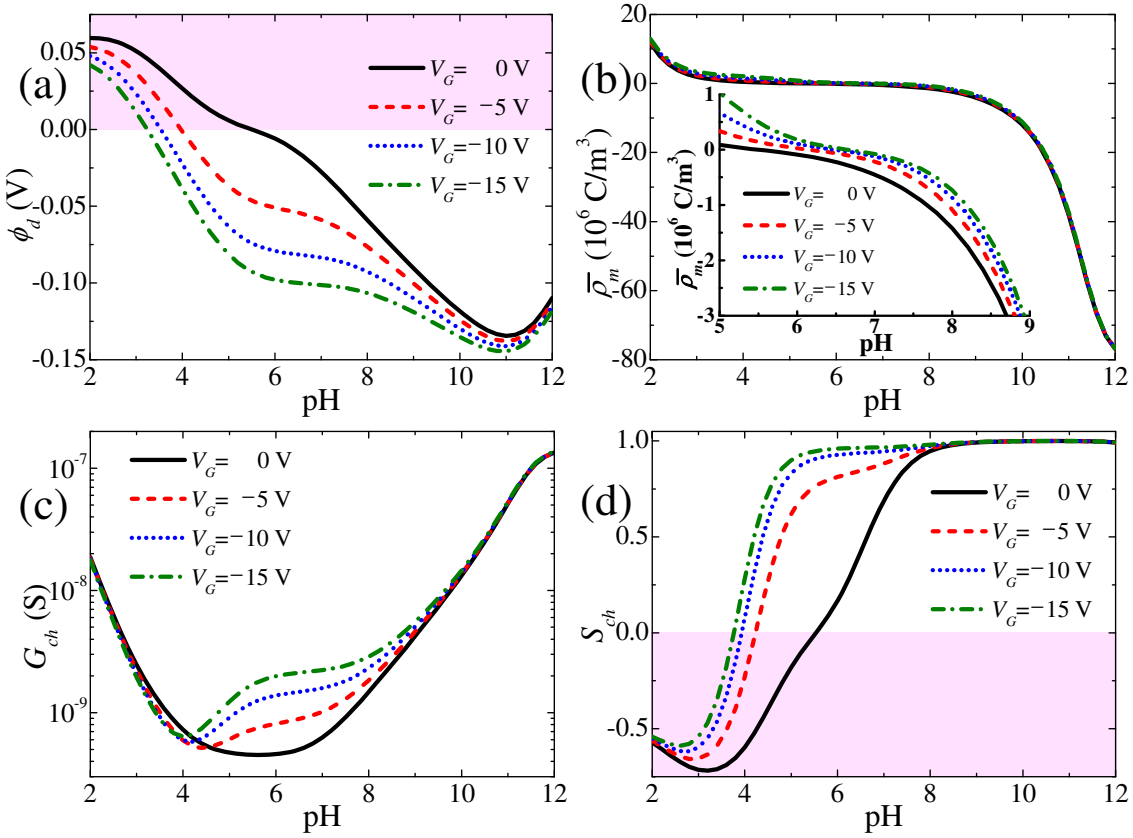

Fig. 5. Donnan potential ϕ_d, (a), volume-averaged charge density of PE brush layers $\bar{\rho}_m$, (b), conductance G_{ch}, (c), and ion selectivity S_{ch}, (d), as a function of pH for various applied gated voltages V_G at $C_b = 1$ mM. The inset in (b) highlights the region for pH in the range of 5 and 9. The pink regions in (b) and (d) highlight where $\phi_d > 0$ and $S_{ch} < 0$, respectively.

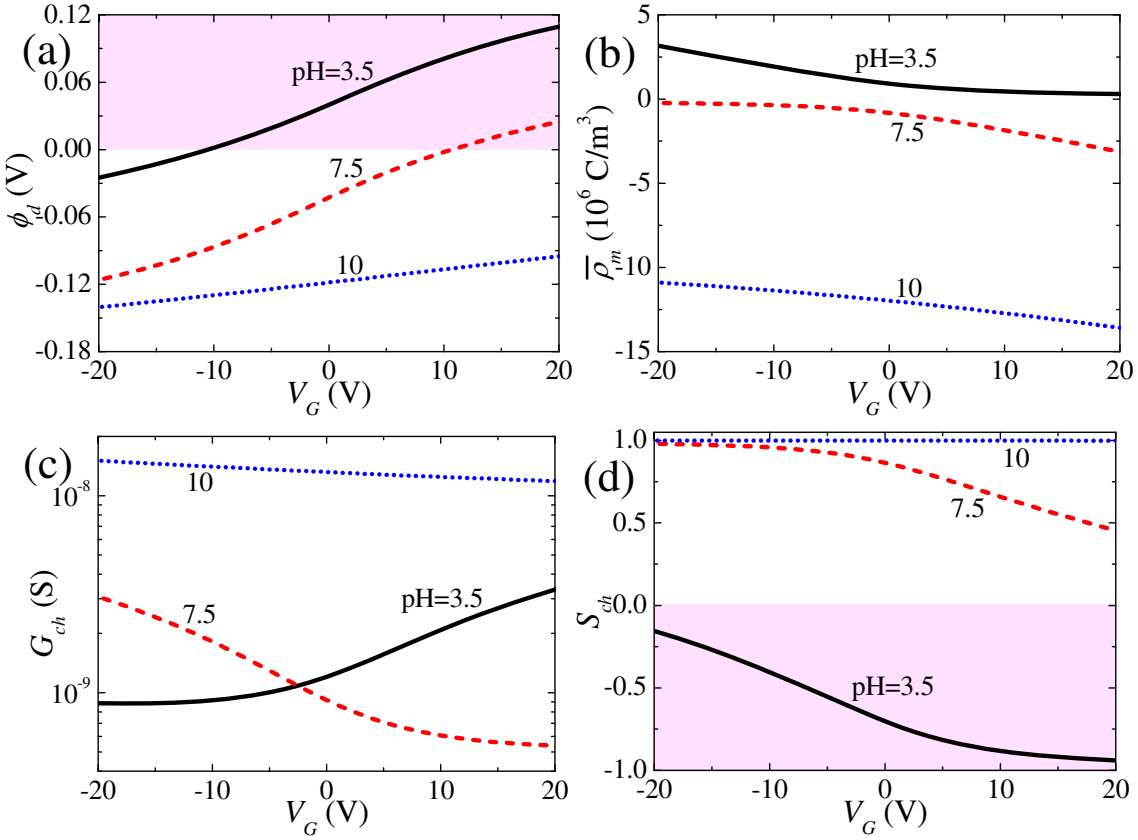

Fig. 6. Gate modulation of the Donnan potential ϕ_d, (a), volume-averaged charge density of PE brush layers $\overline{\rho}_m$, (b), conductance G_{ch}, (c), and ion selectivity S_{ch}, (d), as a function of the applied gated voltage V_G for various pHs at $C_b = 1$ mM. The pink regions in (b) and (d) highlight where $\phi_d > 0$ and $S_{ch} < 0$, respectively.

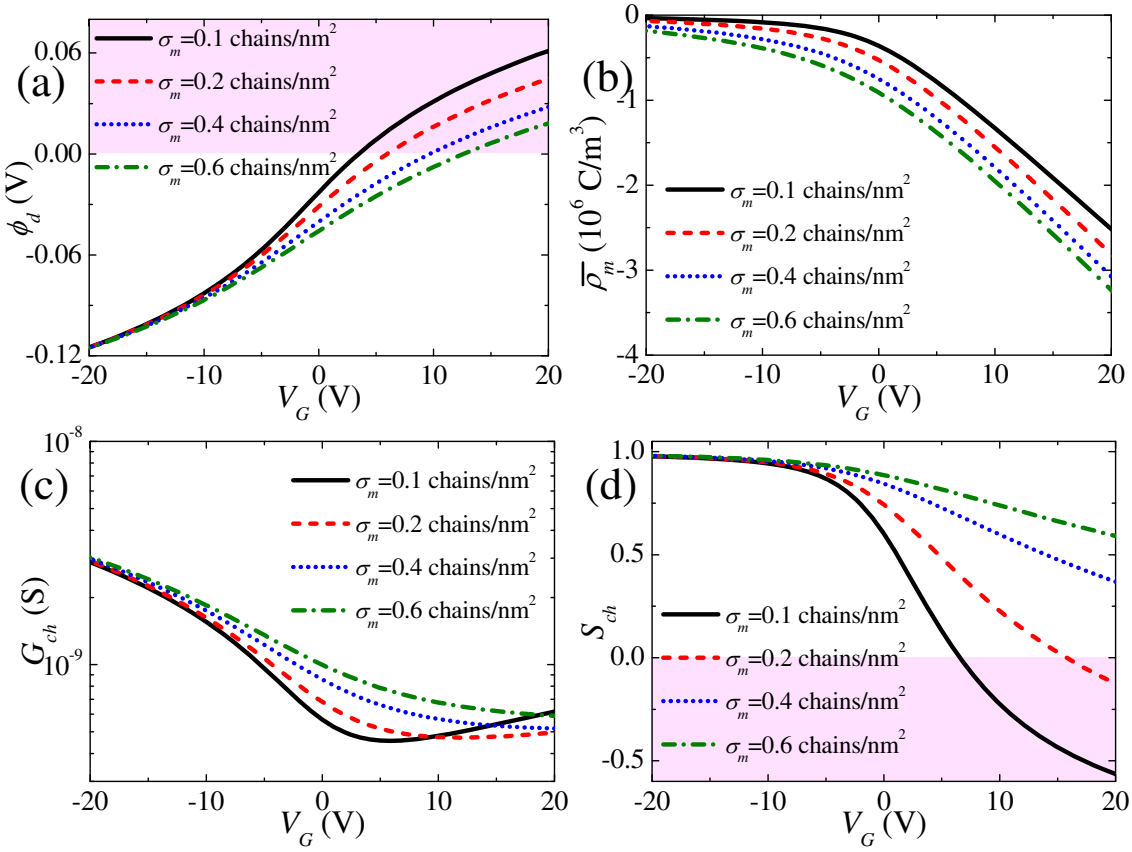

Fig. 7. Gate modulation of the Donnan potential ϕ_d, (a), volume-averaged charge density of PE brush layers $\overline{\rho}_m$, (b), conductance G_{ch}, (c), and ion selectivity S_{ch}, (d), as a function of the applied gated voltage V_G for various grafting density of PE brushes on the inner channel walls at $C_b = 1$ mM and pH = 7. The pink regions in (b) and (d) highlight where $\phi_d > 0$ and $S_{ch} < 0$, respectively.

Graphic Abstract